Summer sea ice floe size distribution in the Arctic: High-resolution optical satellite imagery and model evaluation

Yanan Wang[1], Byongjun Hwang[1], Adam W. Bateson[2], Yevgeny Aksenov[3], Christopher Horvat[4, 5]

[1]School of Applied Sciences, University of Huddersfield, Huddersfield, HD1 3DH, UK
[2]Centre for Polar Observation and Modelling, Department of Meteorology, University of Reading, Reading, RG2 7PS, UK
[3]National Oceanography Centre Southampton, Southampton, SO14 3ZH, UK
[4]Brown University, Providence, USA
[5]University of Auckland, Auckland, NZ

Supplementary Materials

Contents of this file

S1 Perimeter density

In this study, we use the perimeter density per unit ice area P_i (units: m^{-1}) to evaluate the model performance, as it reduces the impacts of partially captured floes at the edge of the image for the FSD retrieval (Perovich, 2002; Perovich and Jones, 2014). There are a number of ways to calculate P_i. In the following, we describe how the FSD models calculate P_i, as well as how P_i can be calculated from the observational FSD data.

Calculation of P_i in the FSD models

In FSD models, P_i is calculated from number FSD n_i distributed into floe size categories i as follows:

$$P_i = \frac{\sum_{i=1}^{12}(2\gamma r_i n_i(r_{i_{max}} - r_{i_{min}}))}{c_{ice}}, \quad (1)$$

where r_i, $r_{i_{max}}$ and $r_{i_{min}}$ are the midpoint, upper and lower limit for each floe size category i. n_i (m^{-3}) is the average number FSD for floe size category i. Here γ is a floe shape parameter, for example $\gamma = 1$ is the assumption of square floes, $\gamma = \pi$ is for circular floes. From the analysis of MEDEA-derived FSD results, the mean floe shape parameter γ is 2.27 in the Chukchi Sea region and 2.23 in the Fram Strait region, respectively. c_i represents the area-weighted sea ice concentration in the selected region.

The areal FSD $f(r)$ and number FSD $n(r)$ are related by

$$f(r) = \gamma r^2 n(r). \quad (2)$$

We can also relate the areal FSD $f(r)$ and CFND $N(r)$ by

$$\int_{r_0}^{\infty} f(r)dr = \int_{r_0}^{\infty} \gamma r^2 dN(r), \quad (3)$$

where r_0 is the lowest cut-off of floe size r. In the prognostic models (FSDv2-WAVE and CPOM-FSD), P_i is calculated from the areal FSD for floe size category f_i (m^{-1}). By combining Eqs. (1) and (2), P_i for prognostic model P_{i_prog} can be calculated by

$$P_{i\_prog} = 2\sum_{i=1}^{12} \frac{f_i(r_{i_{max}} - r_{i_{min}})}{r_i c_{ice}}. \quad (4)$$

For WIPoFSD model, a truncated power law FSD is applied,

$$n(r|r_{min} \le r \le r_{var}) = cr^{-\alpha}, \quad (5)$$

where, r_{min} is the minimum floe radius within floe size categories. The power-law exponent α value used in this study is set to 2.56. The floe size parameter r_{var} varies between r_{min} and the maximum floe radius r_{max} in response to four FSD evolution processes described by Bateson et al. (2020, 2022). The normalization constant c can be defined from that the integral of areal FSD over all floe sizes equal to the fraction of sea ice,

$$\gamma \int_{r_{min}}^{r_{var}} n(r) r^2 dr = c_i \quad (6)$$

$$\text{Hence } c = \frac{(3-\alpha)c_i}{({r_{var}}^{3-\alpha} - {r_{min}}^{3-\alpha})\gamma} \quad (7)$$

P_i for WIPoFSD can be calculated from

$$P_{i\_wipofsd} = \frac{\int_{r_{min}}^{r_{var}} 2\gamma r n(r) dr}{c_{ice}} = \frac{2(3-\alpha)({r_{var}}^{2-\alpha} - {r_{min}}^{2-\alpha})}{(2-\alpha)({r_{var}}^{3-\alpha} - {r_{min}}^{3-\alpha})}. \quad (8)$$

In this study, we used daily outputs from the FSD models to calculate P_i. To obtain P_i from the daily model outputs, we calculated an area-weighted mean, on the same date as the observations, over the grid cells within the study areas of the Chukchi Sea and the Fram Strait.

Calculation of P_i from the observations

To ensure matching with the model outputs, the FSD observation data were binned into the same 12 floe size categories used by the FSD models (Gaussian spacing). By deriving the number of all floes with effective floe radius $r = \sqrt{\frac{a}{\pi}}$ (Horvat and Tziperman, 2015), the radius of a circle that has the same area as a floe, within every floe size category, the average number FSD for each floe size category n_i can be calculated by

$$n_i = \frac{N_i}{A_{ocean}(r_{i_{max}} - r_{i_{min}})}, \quad (9)$$

where N_i is the number of floes with radius between $r_{i_{min}}$ and $r_{i_{max}}$ in the image covering an ocean area of A_{ocean} (units: m2) with floe radius between $r_{i_{min}}$ and $r_{i_{max}}$.

Similarly, the average areal FSD for floe size category f_i can be calculated by

$$f_i = \frac{A_{floe_i}}{A_{ocean}(r_{i_{max}} - r_{i_{min}})}. \quad (10)$$

A_{floe_i} is the area of floes with radius between $r_{i_{min}}$ and $r_{i_{max}}$ in the image.

Now based on the equations described above, we can calculate P_i from the observations using three different methods. From Eqs. (3) and (9), we can produce perimeter density per unit sea ice area from observations using the number FSD,

$$P_{i\_obs1} = \frac{\sum_{i=1}^{12}(2\gamma r_i N_i)}{A_{ice}}, \quad (11)$$

where A_{ice} is the total area of sea ice within the image.

Based on Eqs. (4) and (10), the perimeter density can be calculated by,

$$P_{i\_obs2} = \sum_{i=1}^{12} \frac{2A_{floe_i}}{r_i A_{ice}}. \quad (12)$$

Additionally, we can calculate the floe perimeter density directly from our images,

$$P_{i\_obs3} = \frac{p_{floe}(r_{1_{min}} < r < r_{12_{max}})}{A_{ice}}, \quad (13)$$

where p_{floe} is the total perimeter of floes with radius between $r_{1_{min}}$ and $r_{12_{max}}$ in the image. In Sect. S2, we will test the sensitivity of calculating the perimeter density using Eqs. (11), (12) and (13).

S2 Sensitivity to the floe size category binning and P_i calculation methods.

In this section, we check the sensitivity of calculating P_i for different binning methods and different P_i calculation methods (Eqs. (11), (12) and (13) in Sect. S1). To test the sensitivity of the binning methods, we organised the observational FSD data into four different binning methods: 12 Gaussian-spaced bins, 24 Gaussian-spaced bins, 12 evenly spaced bins, and 24 evenly spaced bins. For the binning, we discarded any ice floes with the effective radius smaller than 0.1 m or larger than 951 m.

Figure S1 shows the results in the relationship between P_i and SIC. As can be seen in Figure S1, the P_i values from evenly spaced binning methods are very sensitive to the different P_i calculation methods (Figure S1c and d). On the other hand, the P_i values from Gaussian spaced binning methods are much less sensitive to the different P_i calculation methods and there are very small differences in the sensitivities between 12 Gaussian spaced binned data and 24 Gaussian spaced binned data (Figure S1a and S1b). Among the three different P_i calculation methods, P_{i_obs2} (Eq. (12), estimated using the floe area) shows the smallest variation throughout the four different binning methods. Based on this, we selected P_{i_obs2} to calculate P_i and use it as the metric for the model-observation comparison and the 12 Gaussian-spaced binning method to match with the model configuration in Roach et al. (2018a) and Bateson et al. (2022).

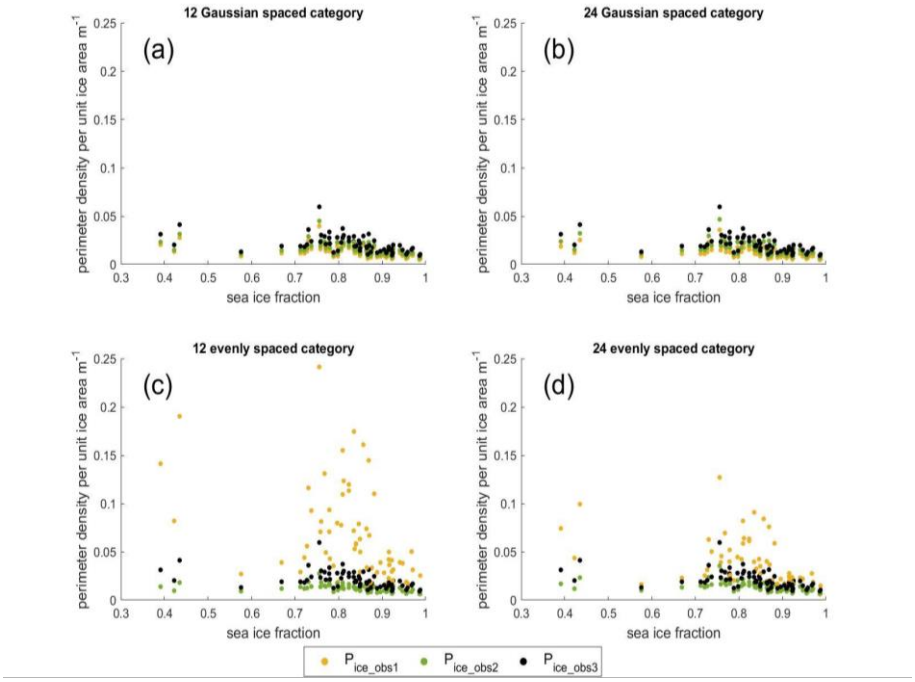

Figure S1. Relationship between perimeter density per unit ice area and SIC for (a) 12 Gaussian-spaced binning, (b) 24 Gaussian-spaced binning, (c) 12 evenly spaced binning, and (d) 24 evenly spaced binning. The perimeter density has been calculated by Eq. (11) (P_{i_obs1}, yellow scatter), Eq. (12) (P_{i_obs2}, green scatter) and Eq. (13) (P_{i_obs3}, black scatter).

Table S1. Difference in P_i (km^{-1}) of small floes within floe size category 1 and 2 (r <14.29) between models and observations in the Chukchi Sea region and the Fram Strait region.

	FSDV2-WAVE		**CPOM-FSD**		**WIPOFSD**	
	CS[a]	**FS[b]**	**CS**	**FS**	**CS**	**FS**
May	132.28	186.44	45.79	71.05	94.91	106.25
June	113.14	179.92	46.47	41.93	93.70	107.29
July	50.27	92.74	33.99	17.60	92.86	110.47
August	/	28.93	/	17.42	/	124.40
Mean	98.56	122.01	42.08	37.00	93.83	112.10

[a] Chukchi Sea.

[b] Fram Strait.

References

Bateson, A. W., Feltham, D. L., Schröder, D., Hosekova, L., Ridley, J. K., and Aksenov, Y.: Impact of sea ice floe size distribution on seasonal fragmentation and melt of Arctic sea ice, Cryosph., 14, 403–428, https://doi.org/10.5194/tc-14-403-2020, 2020.

Bateson, A. W., Feltham, D. L., Schröder, D., Wang, Y., Hwang, B., and Jeff, K.: Sea ice floe size: its impact on pan-Arctic and local ice mass, and required model complexity, Cryosph. [accepted], 2022.

Perovich, D. K.: Aerial observations of the evolution of ice surface conditions during summer, J. Geophys. Res., 107, 8048, https://doi.org/10.1029/2000JC000449, 2002.

Perovich, D. K. and Jones, K. F.: The seasonal evolution of sea ice floe size distribution, J. Geophys. Res. Ocean., 119, 8767–8777, https://doi.org/10.1002/2014JC010136, 2014.

Roach, L. A., Horvat, C., Dean, S. M., and Bitz, C. M.: An Emergent Sea Ice Floe Size Distribution in a Global Coupled Ocean-Sea Ice Model, J. Geophys. Res. Ocean., 123, 4322–4337, https://doi.org/10.1029/2017JC013692, 2018a.